Applied Acoustics 250 (2026) 111337

Contents lists available at ScienceDirect

Applied Acoustics

journal homepage: www.elsevier.com/locate/apacoust

Verification of statistical wave field theory reverberation time predictions

Albert G. Prinn [a,*], Roland Badeau [b]

[a] International Audio Laboratories Erlangen (A joint institution of the Friedrich-Alexander-University (FAU) and Fraunhofer IIS), Am Wolfsmantel 33, Erlangen, 91058, Germany

[b] Laboratoire Traitement et Communication de l'Information, Télécom Paris, Institut Polytechnique de Paris, 19 place Marguerite Perey, Palaiseau, 91120, France

HIGHLIGHTS

- Verification of the statistical wave field theory.
- Estimation of surface impedance in measured rooms.
- Indirect validation of the statistical wave field theory.

GRAPHICAL ABSTRACT

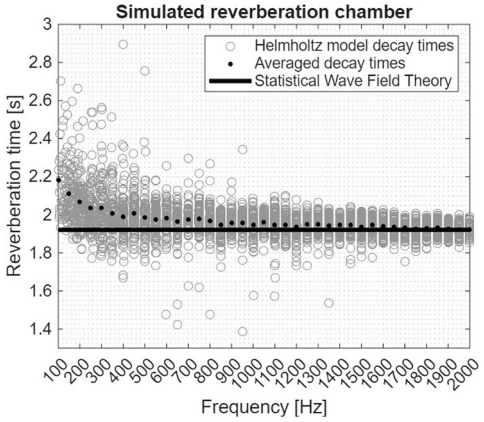

ARTICLE INFO

Keywords:
Statistical wave field theory
Reverberation time
Verification of theory
Impedance estimation

ABSTRACT

Classical statistical reverberation models, such as Sabine's and Eyring's models, provide practitioners with efficient estimates of a room's reverberation time based on its volume, surface area, and the absorption coefficients of its boundary surfaces. Absorption coefficients quantify sound absorption in terms of energy, which can be of limited use when detailed descriptions of interior acoustic fields are required. In such cases, describing absorption in terms of impedance or admittance is preferable. A statistical theory of wave fields has recently been proposed in the literature. The statistical wave field theory predicts reverberation time at high frequencies based on the locally reacting impedances of the surfaces present in a room. This study verifies the predictions of the statistical wave field theory using various numerical models. Additionally, predictions of the theory are indirectly validated by using the theory to estimate surface impedances from measured data, which are in turn used to predict reverberation times in a shoebox-shaped room and in a reverberation chamber.

1. Introduction

Reverberation time is an important parameter in room acoustics. Among various applications, it can be used to assess the acoustic response of a room [1] or to measure the characteristics of sound-absorbing materials [2]. Many models exist that can be used to predict the reverberation time. These models generally fall into one of three categories: numerical wave, geometrical, or statistical models. Numerical

* Corresponding author.
Email address: albert.prinn@fau.de (A.G. Prinn).

https://doi.org/10.1016/j.apacoust.2026.111337
Received 30 November 2025; Received in revised form 9 April 2026; Accepted 13 April 2026
0003-682X/© 2026 The Author(s). Published by Elsevier Ltd. This is an open access article under the CC BY license (http://creativecommons.org/licenses/by/4.0/).

wave models, such as the finite element method, tend to be computationally expensive; however, when provided with precise input parameters, they can be highly accurate. In contrast, geometrical models, like the image source method or the diffusion equation, are more efficient but can be less precise. Statistical models, such as Sabine's formula [3], provide highly efficient predictions, though they tend to be the least accurate.

While the required input parameters for these models may vary, they generally include a description of the room's geometry and the absorption properties of its surfaces. For numerical wave methods and some geometrical methods, surface absorption can be described using complex-valued locally reacting impedance (or its inverse, admittance) or reflection coefficients. In contrast, many geometrical models and most statistical models typically use absorption coefficients to represent sound absorption. The Statistical Wave Field Theory (SWFT), recently proposed by Badeau [4–7], predicts the reverberation time based on the complex-valued, locally-reacting impedance of a room's surfaces. The SWFT offers highly efficient and potentially more accurate predictions of the reverberation time, at least when compared to other statistical models. In this paper, we verify the reverberation time predictions provided by the SWFT using both simulated and measured data.

The paper is organized as follows. A brief introduction to diffuse field theory is provided in Section 2. In Section 3, we present the reverberation time models used to verify the SWFT predictions. In Section 4, we focus on the modal and Helmholtz models that are used to generate reference solutions. Unavoidably, the random incidence absorption coefficient predicted by the SWFT is also included in this section. In Section 5, we compare the reverberation time predictions from these models with those from the SWFT using simulated rooms. In Section 6, we employ the SWFT to estimate the impedances of surfaces in real rooms based on measured data. The estimated impedances are then used as input parameters to diffusion and Helmholtz models of the measured rooms. Good agreement is found between the measured and simulated reverberation times, thereby indirectly validating the SWFT. Conclusions are presented in Section 7.

2. Background

The reverberation time of an acoustic space was first quantified by Sabine in terms of a space's volume, surface area, and absorption coefficient [3]. Eyring improved Sabine's formula by extending it to rooms with short reverberation times [8], i.e., large absorption coefficients. Today, many formulae for reverberation time can be found in the literature (see, e.g., Nowoświat and Olechowska [9], and for a recent review on reverberation time, see Polack [10]). Reverberation time formulae provide efficient predictions that are useful in room and architectural acoustics. The formulae are based on statistical descriptions of a sound field that assume a diffuse field.

A sound field is considered diffuse if: the waves at any receiver position arrive from all directions with equal intensity and random phase. Various definitions can be found in the literature, e.g., those given by Hodgson [11] and Stephenson [12]. While a perfectly diffuse sound field is rarely encountered in practice [13], Martellotta [14] shows that diffuse field theory can provide valuable insights into the propagation of sound in enclosed spaces. Diffuse field theory is applicable in irregularly shaped rooms with uniform absorption and for fields with high modal density (i.e., at high frequencies). Sound fields in reverberation chambers approximate a diffuse field [15].

A diffuse field requires an ergodic and mixing geometry [16,17]. Joyce [18] discusses ergodicity, which can be summarized as the properties of a geometric space that allow a traveling sound particle to explore every location and direction within the space. Joyce also discusses mixing, which describes how traveling particles, initially close to one another, disperse to generate a uniform, isotropic distribution. Mixing is a stronger condition that implies ergodicity. Related to mixing is the mixing time, which is the time at which a room impulse response transitions from a deterministic description to a statistical one.

The variant of SWFT considered here, that is, Ref. [4], makes the following assumptions:

1. the geometric shape of the room is mixing,
2. the frequency of interest is high, i.e., greater than the Schroeder frequency [19], and
3. time is greater than the mixing time, i.e., only late reverberation is considered.

In this work, we model both ergodic and non-ergodic geometries, and we consider both low and high frequencies. We use eigenvalue analyses to simulate sound fields without sources, thereby accounting for a mixing time in the past. We expect the SWFT to hold in most cases, but not all.

3. Reverberation time models

In this verification study, we consider both reverberation time and modal decay time predictions. The modal decay times are computed using a modal model of a shoebox-shaped room and a finite element-based model of the Helmholtz equation for a reverberation chamber. The reverberation times are computed using a finite element-based model of the diffusion equation and the SWFT, for both rooms.

While working in the modal domain may be considered unusual for the verification of a theory that assumes high frequencies and diffuse fields, we will show that there is agreement between the averaged modal decay times and the reverberation times predicted by the SWFT.

3.1. Modal model of a shoebox-shaped room

The modal model of a shoebox-shaped room is based on the theoretical treatment by Morse and Bolt [20]. We would like to compare the modal decay times predicted by this model with the reverberation times given by the SWFT. Thus, we must compute the eigenvalues of the room, from which the modal decay times can be calculated. For a shoebox-shaped room with spatially uniform frequency-independent impedance, ζ, the eigenvalues can be found by solving the three transcendental equations (see, e.g., Kuttruff [21, p. 61])

$$\mathrm{i}k_{n_i} L_i = \ln\left(\frac{k_{n_i}\zeta - k}{k_{n_i}\zeta + k}\right) + \mathrm{i}n_i\pi, \tag{1}$$

where $\mathrm{i} = \sqrt{-1}$, k_{n_i} is the nth eigenvalue in the ith dimension, $n_i \in \mathbb{N}$ is a mode index, $i \in (x, y, z)$, L_i is the length of the room in the ith dimension, and k is the wavenumber. Note that we consider impedances normalized by the characteristic specific acoustic impedance of air, i.e., $\zeta = Z/(\rho_0 c_0)$, where Z is the locally-reacting surface impedance, ρ_0 is the density, and c_0 is the speed of sound. The room's eigenvalues are given by

$$k_n = \sqrt{k_{n_x}^2 + k_{n_y}^2 + k_{n_z}^2}, \tag{2}$$

with approximate solutions given by [20, Eq. (5.5)]

$$k_{n_i} = \begin{cases} \sqrt{\dfrac{2\mathrm{i}k_\mathrm{h}\beta}{L_i}}\left(1 - \dfrac{\mathrm{i}\pi^2 k_\mathrm{h}\beta}{12L_i}\right), & n_i = 0 \\ \dfrac{n_i\pi}{L_i} + \dfrac{2\mathrm{i}k_\mathrm{h}\beta}{\pi n_i} + \dfrac{4k_\mathrm{h}^2\beta^2}{\pi^3 L_i n_i^3}, & n_i > 0 \end{cases} \tag{3}$$

where $\beta = 1/\zeta$ is the normalized surface admittance. The rigid-walled eigenvalues are given by $k_\mathrm{h}^2 = \sum_i \left(\pi n_i/L_i\right)^2$. In the case of a shoebox-shaped room, three mode types can be identified: axial, tangential, and oblique. The eigenvalues of the axial modes are obtained when only one entry of the trio $[n_x,\ n_y,\ n_z]$ is non-zero. When two entries are non-zero, the eigenvalues of the tangential modes are obtained, and when all entries are non-zero, the oblique modes are obtained.

The nth damping constant is given by $\delta_n = \mathrm{Im}(c_0 k_n)$. For the nth damping constant, the modal decay time is given by

$$\mathrm{M}_{60,n} = \frac{3\ln(10)}{\delta_n}, \tag{4}$$

and for a large set of damping constants, the reverberation time is given by [21, Eq. (3.70)]:

$$\mathrm{M}_{60} = \frac{3\ln(10)}{\langle\delta\rangle}, \tag{5}$$

where $\langle\delta\rangle$ indicates an average over several damping constants.

3.2. Finite element-based helmholtz model

The finite element method can be used to predict sound fields in rooms with complex geometries and spatially non-uniform wall impedance. In this work, we use the finite element method to solve the Helmholtz equation. The discretized Helmholtz equation is given by

$$\left[\mathbf{K} + \sum_{j=1}^{J}\left(\frac{\mathrm{i}\omega}{c_0\zeta_j}\mathbf{C}_j\right) - \frac{\omega^2}{c_0^2}\mathbf{M}\right]\mathbf{p} = \mathbf{f}, \tag{6}$$

where subscript j indicates that the surface impedance can be spatially non-uniform, $\omega = 2\pi f$ is the angular frequency, $\mathbf{p}$ is a discretized pressure field, $\mathbf{f}$ is a discretized source condition, and

$$\mathbf{K}_e = \int_e \left(\nabla\mathbf{N}^T \cdot \nabla\mathbf{N}\right)\,\mathrm{d}V_e, \tag{7}$$

$$\mathbf{C}_{e',j} = \int_{e'} \left(\mathbf{N}^T\mathbf{N}\right)\,\mathrm{d}S_{e',j}, \tag{8}$$

$$\mathbf{M}_e = \int_e \left(\mathbf{N}^T\mathbf{N}\right)\,\mathrm{d}V_e, \tag{9}$$

are the elemental stiffness, damping, and mass matrices, respectively. Subscript e represents an interior element with volume V_e, subscript e' represents a boundary element with area $S_{e',j}$, and $\mathbf{N}$ are interpolating shape functions. For brevity, several details have been omitted here. For a derivation of the method, see, e.g., the review by Prinn [22].

The discretized Helmholtz equation can be written as an eigenvalue problem, as follows:

$$\left[\mathbf{K} + \sum_{j=1}^{J}\left(\frac{\lambda}{c_0\zeta_j}\mathbf{C}_j\right) + \frac{\lambda^2}{c_0^2}\mathbf{M}\right]\boldsymbol{\phi} = \mathbf{0}, \tag{10}$$

where λ is an eigenvalue and $\boldsymbol{\phi}$ is the corresponding eigenvector. Solving Eq. (10) for a set of eigenvalues provides predictions of the resonance frequencies

$$f_n = \mathrm{Re}\left(\frac{\lambda_n}{2\pi\mathrm{i}}\right), \tag{11}$$

and damping constants

$$\mu_n = \mathrm{Im}\left(\frac{\lambda_n}{\mathrm{i}}\right). \tag{12}$$

As for the modal model solutions, the modal decay time of the nth mode is given by

$$\mathrm{H}_{60,n} = \frac{3\ln(10)}{\mu_n}, \tag{13}$$

and, given a set of damping constants, $\boldsymbol{\mu}$, the reverberation time is given by

$$\mathrm{H}_{60} = \frac{3\ln(10)}{\langle\boldsymbol{\mu}\rangle}. \tag{14}$$

3.3. Finite element-based diffusion model

The diffusion equation models an almost diffuse field with random incidence absorption coefficients. For a detailed description of the mathematical model, the interested reader is directed toward the derivation by Picaut et al. [23]. In this study, we use the finite element method to discretize the diffusion equation, and write it as the following eigenvalue problem (for derivation see Prinn and Habets [24]):

$$\left[D\,\mathbf{K} + \sum_{j=1}^{J}\left(\frac{c_0\,\overline{\alpha}_j}{2(2-\overline{\alpha}_j)}\mathbf{C}_j\right) - \lambda\mathbf{M}\right]\boldsymbol{\phi} = \mathbf{0}, \tag{15}$$

where we have made use of the modified boundary condition proposed by Jing and Xiang [25]. A typical choice for the diffusion coefficient is

$$D = \frac{l c_0}{3}, \tag{16}$$

given in terms of the mean free path l, which in turn is given by $l = 4V/S$, where V is the room volume and S is the surface area. The random incidence absorption coefficient, $\overline{\alpha}_j$, can be spatially dependent. Solving Eq. (15) for the smallest eigenvalue, λ_s, allows us to estimate the reverberation time of an uncoupled room as follows:

$$\mathrm{D}_{60} = \frac{6\ln(10)}{\lambda_s}, \tag{17}$$

where the additional factor of 2, in comparison with Eqs. (5) and (14), is a consequence of the consideration of energy instead of pressure.

In this work, we specify the impedance; therefore, we need a formula for converting the impedance to the absorption coefficient. We use [21, Eq. (2.11)]:

$$\alpha_j(\theta) = \frac{4\mathrm{Re}(\zeta_j)\cos\theta}{|\zeta_j|^2\cos^2\theta + 2\mathrm{Re}(\zeta_j)\cos\theta + 1}, \tag{18}$$

where θ is the angle of incidence. The random incidence absorption coefficient can be given by the Paris formula [26], which is

$$\overline{\alpha}_{\mathrm{P},j} = \int_0^{\pi/2} \alpha_j(\theta)\sin(2\theta)\,\mathrm{d}\theta. \tag{19}$$

3.4. Eyring formula

While the Sabine formula is a well-known and commonly used reverberation time model, a more accurate formula is the one proposed by Eyring [8]. We will use the following definition in our work:

$$\mathrm{E}_{60} = \frac{24\ln(10)}{c_0}\frac{V}{\sum_{j=1}^{J} -S_j\ln(1-\overline{\alpha}_j)}, \tag{20}$$

where S_j is the surface area of the jth surface.

3.5. Statistical wave field theory

The SWFT offers statistical solutions to the wave equation within a bounded domain. The primary assumptions in its derivation are high frequency and a significant number of reflections, leading to a diffuse field. This theory allows for a closed-form expression of the power distribution of waves over time, frequency, and space, based on the room geometry and specific admittance of the boundary surface.

The SWFT can be used to predict the reverberation time of a room, as follows [4, Eq. (124)]:

$$\mathrm{S}_{60} = \frac{24\ln(10)}{c_0}\frac{V}{\int_{\partial V}\left\{\ln\left(\left|\frac{1+\beta}{1-\beta}\right|^2\right) + 2\mathrm{Re}\left[\beta\left(2-\beta\ln\left(\frac{\beta+1}{\beta-1}\right)\right)\right]\right\}\,\mathrm{d}S}, \tag{21}$$

where $\beta = \beta(S, f)$. For the analyses that follow, we split the surface integral into a sum of integrals over a set of J surfaces, and assume that the admittance of the jth surface is spatially uniform. This allows us to transform the integral into a summation over all surfaces. Thus, we obtain

$$\mathrm{S}_{60} = \frac{24\ln(10)}{c_0} \frac{V}{\sum_{j=1}^{J} \left\{ \left[\ln\left(\left| \frac{1+\beta_j}{1-\beta_j} \right|^2 \right) + 2\mathrm{Re}\left\{ \beta_j \left[2 - \beta_j \ln\left(\frac{\beta_j+1}{\beta_j-1} \right) \right] \right\} \right] S_j \right\}}. \tag{22}$$

Note the similarity to the Eyring formula (20). We will use Eq. (22) to verify the SWFT reverberation time predictions.

Additionally, the SWFT defines a random incidence absorption coefficient [4, Eq. (125)], which can be written in a form that resembles the Paris formula

$$\overline{\alpha}_{\mathrm{S},j} = 1 - \exp\left\{ \int_0^{\pi/2} \ln\left[1 - \alpha_j(\theta)\right] \sin(2\theta)\, \mathrm{d}\theta \right\}, \tag{23}$$

or in closed form,

$$\overline{\alpha}_{\mathrm{S},j} = 1 - \exp\left\{ 2\mathrm{Re}\left[\ln\left(\frac{\zeta_j - 1}{\zeta_j + 1} \right) - \frac{2}{\zeta_j} + \frac{1}{\zeta_j^2} \ln\left(\frac{1+\zeta_j}{1-\zeta_j} \right) \right] \right\}. \tag{24}$$

Using this definition in the Eyring formula, Eq. (20), gives exactly the SWFT solution, while using the Paris formula, Eq. (19), in the Eyring formula gives a different reverberation time prediction for the same impedance. The difference between Eqs. (19) and (24) arises from the use of geometric averaging (in the latter) instead of arithmetic averaging (in the former). The difference becomes apparent for large absorption coefficients, similar to the difference between the Sabine and Eyring formulae. A consequence of this is that, while the Paris formula predicts an absolute maximum absorption coefficient of 0.951 [21], the SWFT predicts a maximum absorption coefficient of 0.992.

3.6. Measures of comparison

Two models are used to generate reference solutions. The modal model provides reference solutions for a shoebox-shaped room, while the Helmholtz model provides reference solutions for a reverberation chamber. The modal model is valid for the entire frequency range; however, as the absorption coefficient approaches unity, the approximation (cf. Eq. (3)) becomes less accurate. The Helmholtz model is also valid for the entire frequency range, but due to limited computational resources, high-frequency Helmholtz solutions are not considered in this work. The highest frequency of the Helmholtz solutions is approximately 2 kHz. Due to the consideration of both low and high frequencies, it is instructive to introduce the Schroeder frequency [19], which is given by

$$f_{\mathrm{Sch}} = 2000\sqrt{\frac{\mathrm{T}_{60}}{V}}, \tag{25}$$

where T_{60} is the reverberation time averaged over all frequency bins. The diffusion model, Eyring formula, and SWFT are valid above the Schroeder frequency.

To quantify the differences between the various models' reverberation time predictions, we use the relative difference

$$R_{\mathrm{I-J}} = \frac{|\mathrm{I}_{60} - \mathrm{J}_{60}|}{\mathrm{I}_{60}} 100, \tag{26}$$

where $\mathrm{I} \in \{\mathrm{M}, \mathrm{H}\}$ and $\mathrm{J} \in \{\mathrm{D}, \mathrm{S}\}$. The differences are computed as a function of either impedance or frequency; this will be stated in the text.

4. Reference models

This section briefly examines the reference solutions provided by the modal and Helmholtz models and identifies the definitions of the absorption coefficient (either Paris or SWFT) and the diffusion coefficient that are used in the diffusion model.

4.1. Modes of a shoebox-shaped room

We consider a shoebox-shaped room with dimensions $L_x = 4$ m, $L_y = 3$ m, and $L_z = 2.5$ m. The speed of sound in the air within the room is $c_0 = 343$ m/s, and the density is $\rho_0 = 1.2$ kg/m^3. The walls of the room have a spatially uniform impedance of $\zeta = 100$.

The modal decay times predicted by the modal model up to 10 kHz are presented in Fig. 1(a). Note, there are more than three million modes below 10 kHz. The decay times of the axial and tangential modes appear in distinct regions. These are determined by the room's dimensions. If all dimensions of the room were equal, only one line for each type of mode would appear. Note that the decay times of the axial modes and some of the tangential modes increase with frequency. This is caused by the wavenumber components for $n_i = 0$ (cf. Eq. (3)). In addition, the decay times for some of the tangential and oblique modes decrease as the frequency increases. This is caused by the second and third terms of the wavenumber components for $n_i > 0$. Thus, for a shoebox-shaped room with frequency-independent impedance, the modal decay times depend on frequency because the discrete wavenumbers are nonlinearly dependent on the rigid-walled wavenumber and the impedance.

According to Kuttruff, the reverberation time is given by an average over all damping constants [21, Eq. (3.70)]. Assuming that this also holds for averages within frequency bands, a frequency-dependent reverberation time for the room can be computed from the modal decay times. This is a simplification of the decay of sound in real space, especially at low frequencies, since we have neglected the spatially dependent amplitudes of the modes (see Prinn et al. [27]). However, since we are interested in solutions of a diffuse field, it is reasonable to assume that the spatially dependent modal amplitudes may be neglected.

4.2. Absorption coefficient definition

With the frequency-dependent reverberation time given by the modal model, we are now in a position to compare the random incidence absorption coefficient predictions (Eqs. (19) and (24)). The Eyring formula can be inverted to provide an estimate of the spatially uniform absorption coefficient as a function of the reverberation time.[1] The Paris and SWFT formulae provide absorption coefficient predictions from knowledge of the normal impedance. Data for three values of impedance are presented in Fig. 1(b). It can be seen that as the frequency increases, the random incidence absorption coefficient predicted by inverting the Eyring formula tends toward the SWFT formula. Additionally, we note that as the impedance increases, the difference between the Paris and SWFT predictions becomes smaller (as stated in Section 3.5).

4.3. Diffusion coefficient definition

The diffusion model includes a diffusion coefficient that may vary across rooms (see, e.g., Fichera et al. [28]). We now determine the diffusion coefficient to use for a diffuse field.

For the reference solution, we use the modal model. However, as shown in Fig. 1(a), at low frequencies the oblique modes approximate the diffuse-field reverberation time. Thus, to reduce computational effort, we choose a reference solution given by the average modal decay time of the first 240 oblique modes, which, for the room considered in this section, implies a maximum frequency of 595 Hz (approximately, since the eigenvalues depend on the impedance). Additionally, instead of comparing the solutions as a function of frequency, we vary the real part of the impedance, i.e., the resistance, from $\zeta = 10$ to $\zeta = 1 \times 10^4$.

The finite element model of the diffusion equation uses quadratic Lagrange shape functions with tetrahedral elements smaller than one-third of the mean free path. We solve the diffusion model with the absorption coefficient definitions given by Eqs. (19) and (24), i.e., $\overline{\alpha}_{\mathrm{P},j}$ and $\overline{\alpha}_{\mathrm{S},j}$, respectively, and we vary the diffusion coefficient.

[1] From Eq. (20), with $J = 1$ and replacing E_{60} with M_{60}, we obtain: $\overline{\alpha} = 1 - \exp\{-24\ln(10)V/c_0\mathrm{M}_{60}S\}$.

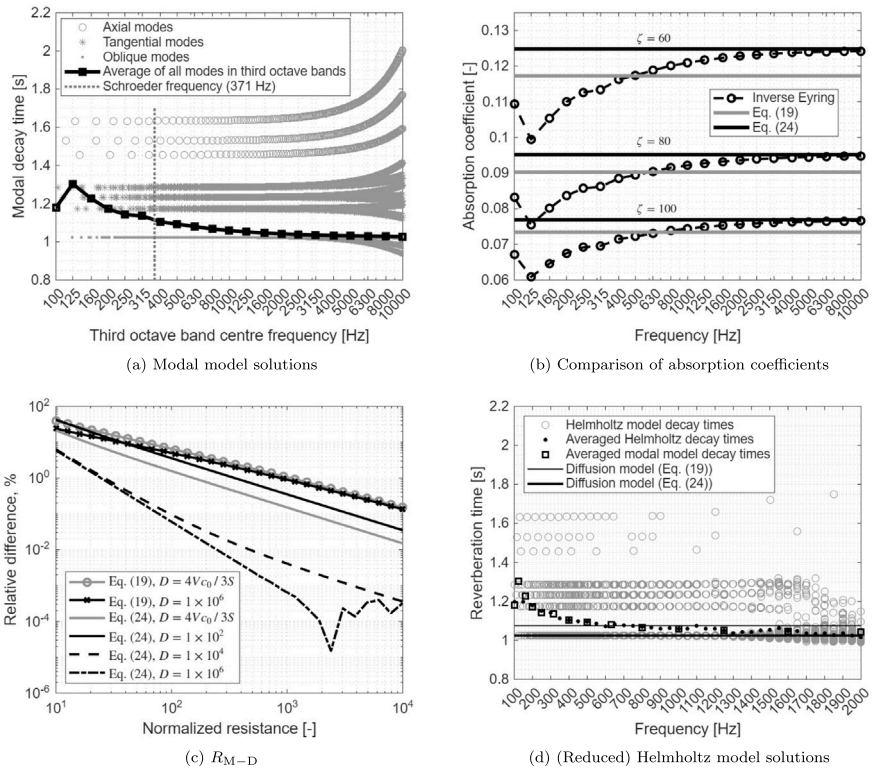

(a) Modal model solutions

(b) Comparison of absorption coefficients

(c) $R_{\mathrm{M-D}}$

(d) (Reduced) Helmholtz model solutions

Fig. 1. Analysis of the reference solutions for the simulated shoebox-shaped room. (a) The modal decay times of a shoebox-shaped room with uniform impedance $\zeta = 100$. The average decay time for each third octave band is included. (b) The absorption coefficients are given by inverting the Eyring formula, Eq. (20), with the average modal decay time as input. Three uniform impedances are considered, $\zeta = 60$, $\zeta = 80$, and $\zeta = 100$, and the predictions by Eqs. (19) and (24) are included. (c) Study of the relative difference between the modal model and the diffusion model predictions, subject to varying absorption and diffusion coefficients. (d) Reverberation time predictions are provided by eigenvalue analyses of a Helmholtz model of the shoebox-shaped room, with $\zeta = 100$. Included are the modal model and diffusion model predictions.

The relative differences, $R_{\mathrm{M-D}}$, obtained by varying the absorption and diffusion coefficients are shown in Fig. 1(c). We observe that all choices of diffusion coefficient provide solutions that converge toward the modal model solution as the resistance increases. When using the absorption coefficient given by Eq. (19), varying the diffusion coefficient does not significantly alter the error as the resistance increases. However, when using the absorption coefficient given by Eq. (24), for large diffusion coefficients, the order of convergence is higher. Therefore, to obtain diffuse field solutions, we choose to use the absorption coefficient given by Eq. (24), i.e., $\overline{\alpha}_j = \overline{\alpha}_{\mathrm{S},j}$ (unless specified otherwise), and a diffusion coefficient of $D = 1\times10^6$. Note that the finite element model of the diffusion equation used here is poorly conditioned, as evidenced by the noise in the convergence plot for $D = 1\times10^6$ above a resistance of approximately $\zeta = 1\times10^3$. Thus, while a larger value of diffusion coefficient might be considered, the poor conditioning places a practical upper limit on the diffusion coefficient.

4.4. Helmholtz model solution

The finite element-based Helmholtz model is used to provide reference solutions for the irregularly shaped room considered in this study. The computational cost of the standard finite element method increases significantly with increasing frequency. Thus, to reduce computational effort in this study, only a subset of room modes is considered (see Appendix A for more details). In this section, we confirm that the modal model and the (*reduced*) Helmholtz model solutions are similar.

Instead of computing all modes of the room, only 100 modes in the region of a *nominal* frequency are computed. The nominal frequencies range from 100 Hz to 2 kHz, in steps of 50 Hz. A tetrahedral mesh with fifth-order (quintic) interpolating shape functions is used, and the size of the largest element in the mesh is defined by specifying a number of degrees of freedom per wavelength, $N_{\mathrm{dof}/\lambda}$. Due to the computational costs of computing the eigenvalues, $N_{\mathrm{dof}/\lambda}$ varies with nominal frequency. These values are reported in Table 2. It is important to note that we use fewer than the recommended $N_{\mathrm{dof}/\lambda}$ at higher frequencies, and despite using quintic interpolation functions, there is some numerical error present in this data.

In Fig. 1(d), the reverberation times obtained by averaging the modal model solutions in each third octave band are compared to the reverberation times found at the nominal frequencies. It can be seen that there is qualitative agreement between the modal model and the (reduced) Helmholtz model solutions.[2] From this observation and the finite element method's ability to provide robust solutions for arbitrarily shaped rooms, we infer that the (reduced) Helmholtz model solutions can serve as reference solutions for irregularly shaped rooms. Also included in the figure is the diffusion model, with $D = 1\times10^6$ solutions obtained using both Eqs. (19) and (24). We observe that the diffusion model with Eq. (24) solution agrees with the oblique mode decay times. Finally, we note that as the frequency increases, the modal model, Helmholtz model, and diffusion model with Eq. (24) appear to converge.

5. Verification

In this verification study, we compare the predicted reverberation times for a simulated shoebox-shaped room and a simulated reverberation chamber.

[2] Note the "spreading" of the decay times with increasing frequency observed in Fig. 1(a) is also present in the (reduced) Helmholtz data presented in Fig. 1(d).

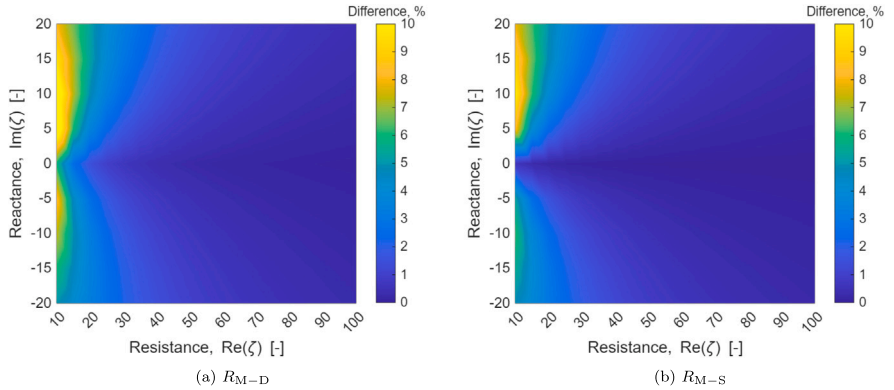

Fig. 2. Comparison of relative differences between the predicted reverberation times for the simulated shoebox room as a function of complex-valued impedance. (a) Diffusion model. (b) SWFT.

Table 1
Coordinates of the corners of the simulated reverberation chamber, given in meters.

	x	y	z
A	0.36	0.82	0.00
B	8.26	0.25	0.00
C	8.08	5.84	0.00
D	0.02	5.87	0.00
E	0.76	0.56	4.33
F	7.86	0.03	4.65
G	7.61	6.20	5.15
H	0.42	6.20	4.78

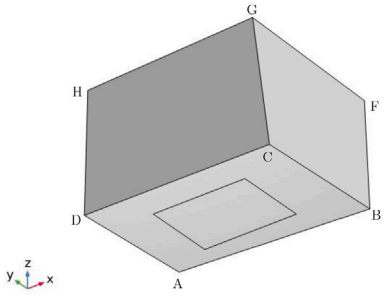

Fig. 3. Simulated reverberation chamber, with a sample placed on the floor. Note: three of the walls have been removed for ease of presentation.

5.1. Shoebox-shaped room

We continue to use the room that was presented in Section 4.1. However, in this case, the complex-valued normalized impedance of the room's walls is varied. The real part of the impedance, the resistance, is varied from 10 to 100, while the imaginary part, the reactance, is varied from -20 to 20.

The modal model is used to generate reference solutions. As for the data presented in Fig. 1(c), the average of the first 240 modal decay times serves as the reference solution. The relative differences of the reverberation time predictions are presented in Fig. 2. In Fig. 2(a), R_{M-D} as a function of resistance and reactance is presented. We observe that when the reactance is small and the resistance is large, the relative difference is small. As the absolute value of the reactance increases, R_{M-D} increases. In general, we observe that R_{M-D} is greater when the absorption is higher, and the impedance is complex-valued. In Fig. 2(b), R_{M-S} is presented. We see that the trend of the differences is similar to that of the diffusion model. This is to be expected since the sound field in a highly damped room will have fewer reflections than that of a lightly damped room, and is thus less likely to approach a diffuse field. The predictions of both models converge toward the reference solution as the damping decreases.

5.2. Reverberation chamber

A simulated reverberation chamber with variable surface impedance is considered in this section. The room's geometry has been designed to ensure the chamber is ergodic. The corner dimensions of the room are provided in Table 1, and the room model is illustrated in Fig. 3. The chamber has a volume of 200.23 m^3 and a surface area of 209.92 m^2. The speed of sound in the air in the chamber is $c_0 = 343$ m/s, and the density is $\rho_0 = 1.2$ kg/m^3. Eigenvalue analysis of the finite element-based Helmholtz model is used to generate the reference solutions. As discussed in Section 4.4, due to high computational costs, subsets of all possible modes at nominal frequencies are computed. The reference reverberation times are computed by averaging a set of modal decay times.

In this section, we present the relative differences between the Helmholtz and diffusion, and the Helmholtz and SWFT models, for an empty chamber and an occupied chamber, i.e., a spatially uniform impedance and a spatially non-uniform impedance, respectively.

5.2.1. Spatially uniform impedance

We compare the Helmholtz and SWFT reverberation time predictions as a function of frequency, for a spatially and frequency-independent impedance of $\zeta = 100$. This data is shown in Fig. 4(a). We observe that at low frequencies, the modal decay times have a larger range than those at high frequencies. As the frequency increases, the range diminishes, and the Helmholtz and SWFT predictions converge. The diffusion model predictions with the Paris formula are also presented. In this case, the use of the Paris formula underpredicts the absorption coefficient.

Next, we consider the relative differences R_{H-D} and R_{H-S} as a function of varying complex-valued impedance.[3] This data is given in Fig. 5(a) and (c), respectively. We observe that as the resistance increases R_{H-D} and R_{H-S} decrease. The differences are greatest for small values of resistance and reactance, and in this case, R_{H-S} is slightly higher than R_{H-D}. As impedance decreases, the differences increase because the sound field under test becomes less diffuse. In general, we

[3] To reduce computational effort, for each instance of complex-valued impedance, 50 eigenvalues in the region of a nominal frequency of 1 kHz are used to compute H_{60}.

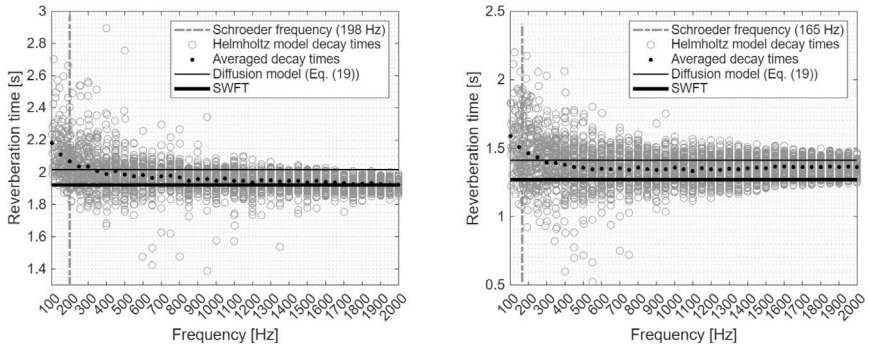

(a) Uniform impedance (b) Non-uniform impedance

Fig. 4. Comparison of reverberation time predictions in the simulated reverberation chamber.

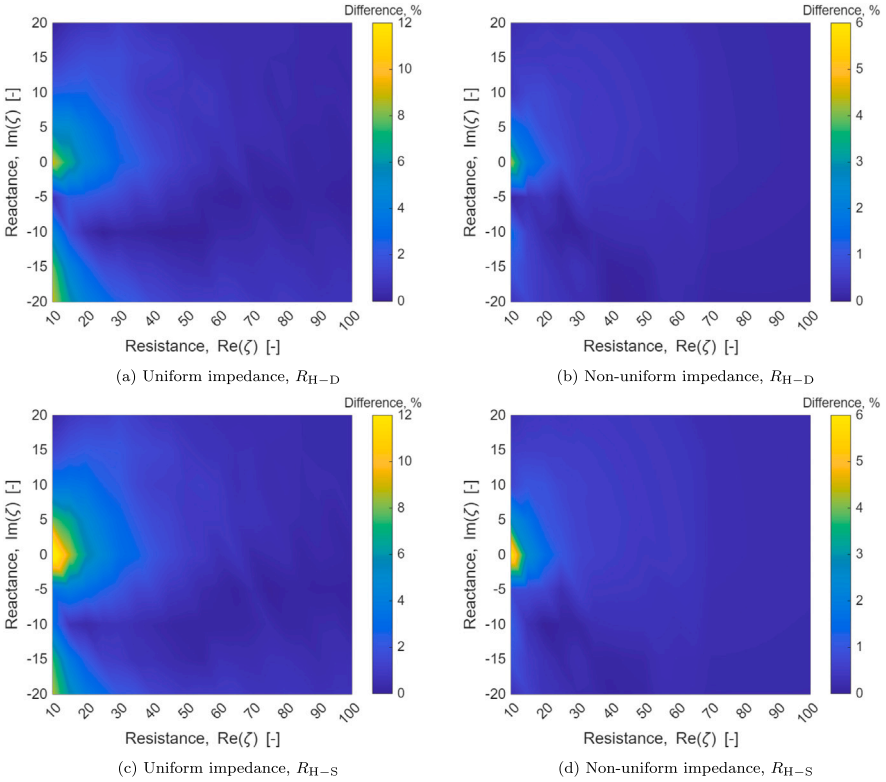

(a) Uniform impedance, $R_{\mathrm{H-D}}$ (b) Non-uniform impedance, $R_{\mathrm{H-D}}$

(c) Uniform impedance, $R_{\mathrm{H-S}}$ (d) Non-uniform impedance, $R_{\mathrm{H-S}}$

Fig. 5. Relative differences as a function of complex-valued impedance in the simulated reverberation chamber for spatially uniform impedance (empty chamber) and spatially non-uniform impedance (occupied chamber).

observe that the Helmholtz and SWFT predictions appear to converge as the impedance increases.

5.2.2. Non-uniform impedance

Let us again consider the Helmholtz and SWFT predictions as a function of frequency, but this time for spatially non-uniform impedance. In this case, we consider a reverberation chamber with a sample placed on the floor (depicted in Fig. 3). The sample is flush to the floor, and has a length of 4 m, and a width of 3 m. The walls of the chamber have a constant impedance of $\zeta_w = 100$, and the impedance of the sample on the floor is $\zeta_s = 10$. From Fig. 4(b), it can be seen that as the frequency increases, the Helmholtz model predictions lie between the SWFT and diffusion model with the Paris formula predictions. While this reverberation chamber is ergodic, it is not mixing and is only approximately diffuse. We expect the non-uniform impedance to further degrade its diffusivity. Thus, in this case, the assumptions of the SWFT are less satisfied than in the uniform case.

To compute the relative differences as a function of impedance, we vary the sample's complex-valued impedance. The resistance is varied from 10 to 100, and the reactance is varied from -20 to 20.[4] Relative differences $R_{\mathrm{H-D}}$ and $R_{\mathrm{H-S}}$ are presented in Fig. 5(b) and (d), respectively. The differences between the diffusion model and the SWFT model are similar. In general, as the impedance increases $R_{\mathrm{H-D}}$ and $R_{\mathrm{H-S}}$ decrease.

5.3. Convergence

The relative difference between the Helmholtz data presented in Fig. 1(d) and the SWFT predictions, and the difference between the data presented in Fig. 4(a) are presented in Table 2. This data verifies that in the shoebox-shaped room and reverberation chamber with uniform

[4] For each impedance, reference solutions are obtained from an average of 50 eigenvalues in the region of a nominal frequency of 1 kHz.

Table 2
Relative differences between the Helmholtz and SWFT models for increasing frequency. Also included are the number of degrees of freedom per wavelength used for each finite element model.

Nominal frequency [Hz]	Shoebox, Fig. 1(d) $R_{\mathrm{H-S}}$ (%)	Empty, Fig. 4(a) $R_{\mathrm{H-S}}$ (%)	Occupied, Fig. 4(b) $R_{\mathrm{H-S}}$ (%)	$N_{\mathrm{dof}/\lambda}$
100	14.59	11.94	20.10	57
150	14.49	8.98	15.72	38
200	13.14	7.03	13.11	28
250	11.09	5.57	11.27	23
300	10.33	5.65	8.96	19
350	7.91	4.35	8.61	16
400	7.26	3.51	7.97	14
450	6.72	4.35	6.83	13
500	6.50	3.31	6.35	11
550	5.74	2.77	5.71	10
600	4.49	3.03	5.89	9
650	5.41	2.29	5.64	9
700	4.96	2.72	6.17	8
750	4.77	2.85	5.27	8
800	4.07	2.34	6.54	7
850	3.95	1.30	5.63	7
900	3.27	1.90	5.21	6
950	3.52	1.84	5.55	6
1000	3.37	1.28	6.34	6
1050	3.32	2.05	5.67	5
1100	4.66	1.26	4.81	5
1150	3.30	1.34	6.21	5
1200	3.42	0.78	5.64	5
1250	2.62	1.49	5.30	5
1300	1.15	1.49	5.99	4
1350	1.69	1.15	5.61	4
1400	1.83	1.36	6.25	4
1450	2.59	1.27	6.31	4
1500	2.87	0.74	6.10	4
1550	3.52	1.29	6.91	4
1600	2.23	1.01	6.96	4
1650	2.27	0.69	6.84	3
1700	1.15	0.55	6.71	3
1750	0.83	0.14	6.82	3
1800	1.26	0.34	6.71	3
1850	0.19	0.57	7.10	3
1900	1.23	0.24	6.72	3
1950	0.02	0.09	6.89	3
2000	0.85	0.04	6.63	3

impedance, the SWFT reverberation time predictions converge toward the average of the modal decay times of the Helmholtz equation as the frequency increases. The difference of the data presented in Fig. 4(b), also presented in Table 2, shows that for the reverberation chamber with spatially non-uniform impedance, while $R_{\mathrm{H-S}}$ is low, it does not decrease with increasing frequency. In this case, the SWFT predicts a lower reverberation time than the Helmholtz model. The data presented in Fig. 5 show that the SWFT predictions approach the Helmholtz solutions as the impedance increases, for both uniform and non-uniform impedance.

6. Indirect validation

To further verify the SWFT, we use the theory to estimate the impedances of surfaces in measured rooms. We then use these estimated impedances as input parameters for diffusion and Helmholtz models, and compare the average measured and predicted reverberation times. This study provides an indirect validation of the SWFT. The study focuses on two types of rooms: an approximately shoebox-shaped room and a reverberation chamber.

6.1. Shoebox-shaped room

6.1.1. Room and measurement description

A photograph of the room under test is given in Fig. 6(a). Although the room is approximately shoebox-shaped, it features several sound-scattering elements. For example, there are two recessed windows on one wall, and pipes and cables run along the ceiling. We choose to omit these elements and model the room as a shoebox with dimensions $L_x = 9.56$ m, $L_y = 3.80$ m, and $L_z = 2.54$ m. The room has a volume of 92.27 m^3 and a surface area of 140.52 m^3. The speed of sound in the room is $c_0 = 340$ m/s, and the density is $\rho_0 = 1.2$ kg/m^3. The walls, floor, and ceiling visible in Fig. 6(a) are painted concrete surfaces and are assumed to have the same impedance (including the mirror on the right). The wall not in the photograph is made of plasterboard and is assumed to have an impedance different from that of the other walls. Thus, the room has a long reverberation time and spatially non-uniform impedance.

A loudspeaker is placed in one corner of the room and excited with an exponentially swept sine signal [29]. The resulting acoustic field is captured at 12 receiver positions. The measured signals are deconvolved to obtain 12 measured room impulse responses. The measured reverberation time is presented in Fig. 6(b).

6.1.2. Impedance estimation

For each measured impulse response, the reverberation time as a function of third-octave frequency bands is computed.[5] From this data, we aim to estimate two complex-valued impedances, i.e., $J = 2$. The

[5] Using a second-order Butterworth filterbank, Schroeder integration [30] of the resulting narrow-band impulse responses, and extrapolation of straight line fits to the energy decay curves between -5 and -25 dB.

(a) Photograph of the measured room

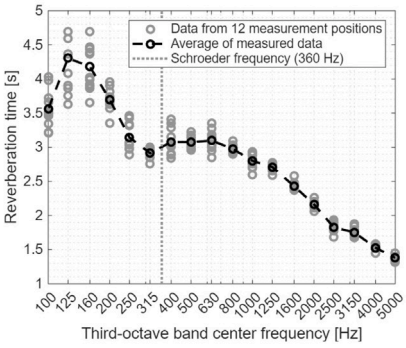

(b) Measured and averaged reverberation times

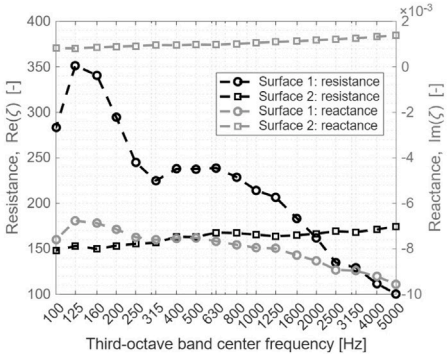

(c) Estimated impedances of the two main surfaces

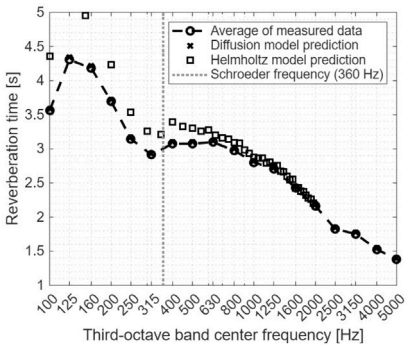

(d) Averaged and simulated reverberation times

Fig. 6. Presentation of the measured shoebox-shaped room, with estimates of the spatially non-uniform impedance obtained using the SWFT model, and predictions of the reverberation time obtained from the diffusion and Helmholtz models.

impedance estimation is written as an optimization problem. For each frequency band, the optimization problem reads

$$\tilde{\boldsymbol{\zeta}}(\omega_c) = \underset{\mathrm{Re}(\hat{\zeta}_1),\ \mathrm{Im}(\hat{\zeta}_1),\ \mathrm{Re}(\hat{\zeta}_2),\ \mathrm{Im}(\hat{\zeta}_2)}{\arg\min} \|\mathbf{T}_{60}(\omega_c) - \widehat{\mathbf{S}}_{60}(\omega_c)\|_2, \tag{27}$$

where $\mathbf{T}_{60}$ is a vector containing the measured reverberation times from the 12 measurement positions, $\widehat{\mathbf{S}}_{60}$ is a vector containing the SWFT prediction repeated 12 times, and ω_c is the center frequency of a given third-octave band. The initial guesses

$$\left[\mathrm{Re}(\hat{\zeta}_1),\ \mathrm{Im}(\hat{\zeta}_1),\ \mathrm{Re}(\hat{\zeta}_2),\ \mathrm{Im}(\hat{\zeta}_2)\right] = [100,\ 0,\ 100,\ 0] \tag{28}$$

are used, and the local minimum of the Euclidean distance between the measured and predicted reverberation times estimates four unknown values representing the complex impedances of the two surfaces. We use MATLAB's fminsearch function [31] to solve Eq. (27).

The estimated resistances and reactances are presented in Fig. 6(c). We observe that two different impedances have been estimated. For both of these impedances, the absolute value of the reactance is of the order of 10^{-3}. Since the surfaces in this room are stiff, as evidenced by the long reverberation times, we expect the reactances of the surfaces to be small. The differences between the estimated resistances indicate the presence of two different types of surfaces, as expected. While these estimates are encouraging, they must be treated with caution. These estimates can vary with the initial guesses and are therefore not unique. We have used measured reverberation times to estimate two complex-valued impedances, which means we have not explicitly included phase, and the optimization problem is underconstrained. We would need to extract additional information from the measured field to constrain the optimization problem and make these estimates unique. Thus, these estimates are only approximations of the actual surface impedances, and there is room for improvement. This is discussed further in Section 6.3.

6.1.3. Comparison of reverberation times

These impedances are converted to absorption coefficients, using the SWFT definition, Eq. (24), and are then used as input parameters for a diffusion model of the room. In this case, the diffusion model uses the standard definition of the diffusion coefficient, i.e., Eq. (16). An eigenvalue analysis of the diffusion model provides predictions of the reverberation times. Additionally, the estimated impedances are used as input parameters for the Helmholtz model. Due to prohibitive computational cost, the highest nominal frequency used for the Helmholtz model is 2 kHz.

The average of the measured reverberation times and the predicted reverberation times is compared in Fig. 6(d). It can be seen that the average measured and diffusion model data are in agreement, but this could be attributed to the similarity of the SWFT and diffusion models. A stricter test of the estimated impedances is using them as input parameters for the Helmholtz model. In this case, there is poor agreement below the Schroeder frequency. Due to low modal density, the poor agreement is to be expected. However, as the frequency increases, the agreement improves, which suggests that at high frequencies the SWFT might provide useful estimates of wall impedance.

6.2. Reverberation chamber

6.2.1. Chamber and measurement description

The reverberation chamber is formed by two reverberant rooms joined by a large, open-windowed area. A sketch of the room is provided in Fig. 7(a). The chamber is either empty or has two material samples placed on the floor, which we will refer to as the *occupied* state. The empty chamber has a volume of 203.11 m^3, and a surface area of 301.34 m^2. The occupied chamber has a volume of 202.27 m^3 and a surface area of 303.58 m^2.

The procedure for measuring the chamber's reverberation time is similar to that used for the shoebox room. That is, a loudspeaker is placed on the floor in one corner of the chamber (as indicated in Fig. 7(a)), and

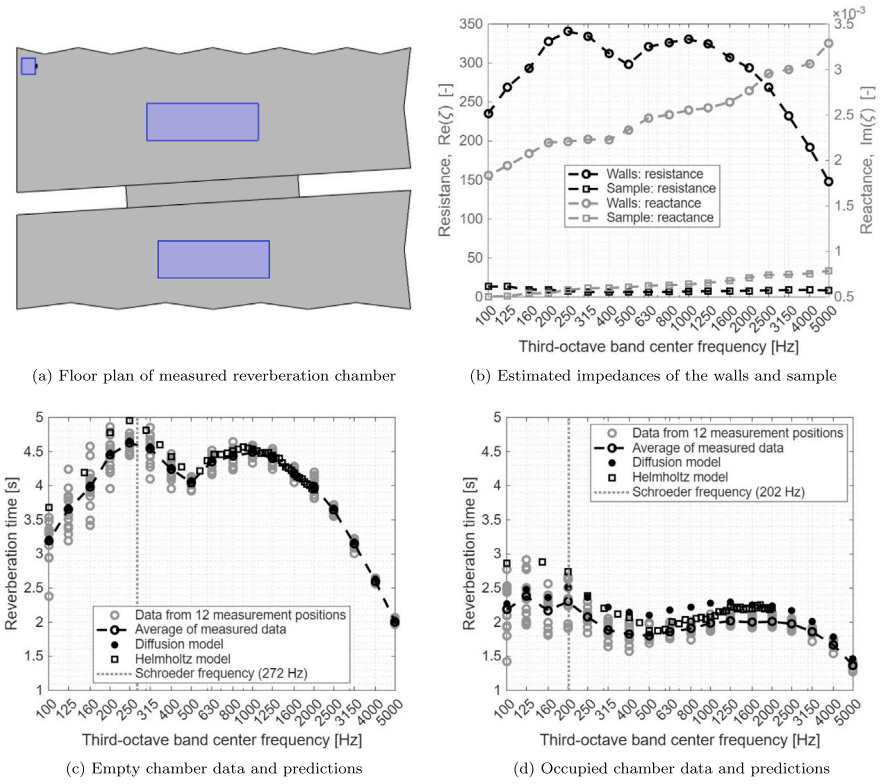

(a) Floor plan of measured reverberation chamber

(b) Estimated impedances of the walls and sample

(c) Empty chamber data and predictions

(d) Occupied chamber data and predictions

Fig. 7. Presentation of the measured reverberation chamber, including loudspeaker position and two samples. Estimates of the wall impedance and sample impedance were obtained using the SWFT model. Predictions of the reverberation times of the empty and occupied chambers are given by the diffusion and Helmholtz models.

room impulse responses are obtained at 12 receiver positions. Two sets of data are measured. One is from the empty chamber, and the other is from the occupied chamber.

6.2.2. Impedance estimation

In this case, the impedance estimation is performed sequentially. First, the SWFT is used to estimate the impedance of the chamber's walls from the 12 impulse responses of the empty chamber. Next, with the knowledge of the chamber wall impedance, we estimate the impedance of the material sample from the 12 impulse responses of the occupied chamber. In comparison to the estimates presented in Section 6.1.2, only one complex-valued impedance is estimated for each frequency. In this case, the optimization problems read

$$\tilde{\boldsymbol{\zeta}}(\omega_c) = \underset{\mathrm{Re}(\hat{\zeta}_j),\ \mathrm{Im}(\hat{\zeta}_j)}{\arg\min} \|\mathbf{T}_{60}(\omega_c) - \hat{\mathbf{S}}_{60}(\omega_c)\|_2, \tag{29}$$

with initial guesses

$$\left[\mathrm{Re}(\hat{\zeta}_j),\ \mathrm{Im}(\hat{\zeta}_j)\right] = [100,\ 0]\,, \tag{30}$$

where $j = 1$ for the empty chamber, and $j = 2$ for the occupied chamber.

The estimated resistances and reactances are presented in Fig. 7(b). We observe that the material sample's resistance is significantly lower than that of the chamber walls, as expected. Additionally, we note that the estimated reactances are of the order of 10^{-3}, and the reactance of the walls is greater than that of the sample, which is unexpected. We reiterate that, since the optimization problem is underconstrained, these data should be understood as approximations of the actual impedance data. Clearly, further validation studies are required.

6.2.3. Comparison of reverberation times

We use the estimated impedances to define absorption coefficients for diffusion models of the empty and occupied chambers, and following eigenvalue analyses of the models, we predict the reverberation times for these two conditions. As for the measured shoebox-shaped room, the diffusion model uses the standard diffusion coefficient and the SWFT absorption coefficient definition. Additionally, the estimated impedances are used as input parameters for the Helmholtz model.

The measured, the average of the measured, and the predicted reverberation times for the empty and occupied chambers are compared in Fig. 7(c) and (d), respectively. The diffusion model predictions of the reverberation time for the empty chamber are in good agreement with the measured data. This is to be expected because the reverberation time is high in the empty chamber, and a diffuse field assumption is reasonable in this case. The Helmholtz model predictions agree with the measured data for higher frequencies, which suggests that the wall impedance is well estimated by the SWFT at high frequencies.

We observe in Fig. 7(d) that the diffusion model data reveal only qualitative agreement, and that using the estimated wall and sample impedances as input data for the Helmholtz model of the occupied reverberation chamber results in reverberation times that are higher than the measured data. Based on the data in Fig. 4(b), which shows that in the nonuniform impedance case the SWFT may underestimate the reverberation time, we expect that the SWFT has overestimated the sample impedance values, thereby causing the Helmholtz model to predict slightly longer reverberation times.

6.3. Discussion

We observe in the measured data that the variance of the reverberation time decreases with increasing frequency, indicating a transition toward a more uniform decay. Noting the good agreement obtained at the high frequencies considered, we expect the SWFT predictions to become more accurate at higher frequencies. In sound fields with low modal density, the SWFT is less applicable. In general, the data are qualitatively consistent, suggesting that, with further

development of the approach, it may be possible to use the SWFT to estimate the normal impedances of surfaces. Possible developments may include:

- measuring the spatial power distribution, and comparing this to the SWFT predictions [4], or
- measuring the sound field using directional microphones, and comparing this data to the SWFT predictions of anisotropic wave fields [7].

However, such extensions lie outside the scope of this study. In summary, when the SWFT assumptions are satisfied, the theory provides reliable predictions of reverberation time. In modal regions and non-diffuse rooms, the agreement is qualitative.

7. Conclusions and future directions

The Statistical Wave Field Theory (SWFT) reverberation time predictions have been compared to solutions of various reverberation time model predictions. For a simulated shoebox room, good agreement between the modal model, diffusion model, and SWFT predictions has been found, both as a function of frequency and as a function of complex-valued impedance. In further support of the veracity of SWFT, good agreement has also been found between the Helmholtz model, the diffusion model, and the SWFT predictions for a simulated reverberation chamber. The convergence of the solutions with increasing frequency and impedance confirms that the SWFT effectively predicts the reverberation time in a diffuse field, based on the room's volume, surface area, and surface impedance. Additionally, the SWFT has been used to estimate the impedance of surfaces in a measured shoebox-shaped room and in a measured reverberation chamber. The agreement between the average measured reverberation times and predictions from the diffusion and Helmholtz models that use the estimated impedances as input parameters indirectly validates the SWFT. In principle, it might be possible to use the SWFT to measure the impedance of surfaces in a room. However, the development and validation of such an approach are left for future studies.

CRediT authorship contribution statement

Albert G. Prinn: Writing – review & editing, Writing – original draft, Methodology, Investigation. **Roland Badeau:** Writing – review & editing, Investigation, Conceptualization.

Declaration of competing interest

The authors declare that they have no known competing financial interests or personal relationships that could have appeared to influence the work reported in this paper.

Acknowledgment

The authors would like to thank Dr. Eduardo Latorre Iglesias and Rubén Maestro Vallejo at Universidad Politécnica de Madrid for the measured reverberation chamber data. The authors would also like to thank the anonymous reviewers for their insightful suggestions. The authors gratefully acknowledge the scientific support and HPC resources provided by the Erlangen National High Performance Computing Center (NHR@FAU) of the Friedrich-Alexander-Universität Erlangen-Nürnberg (FAU). The hardware is funded by the German Research Foundation (DFG).

Appendix A. Reduced Helmholtz model solutions

The number of eigenvalues in a room increases with frequency. This has been quantified for a shoebox-shaped room by Kuttruff [21]. The number of modes given by [21, Eq. (3.29)] is presented in Fig. A.8(a), as a function of mode type, for the room presented in Section 4.1. As the frequency increases, the number of oblique modes dominates the modal field. Additionally, since the oblique modes interact with all surfaces, there tends to be less variation in the oblique mode decay times than there is in the decay times of the axial and tangential modes. This is confirmed upon consultation of Fig. 1(a). Therefore, as the frequency increases, we expect less variation in the modal decay times.

As a measure of the variation of the data used in this work, we make use of the following coefficient of variation

$$C(f_m) = \frac{\sigma}{\mu}, \tag{A.1}$$

where f_m is a nominal frequency, σ is the standard deviation of the modal decay times, and μ is the mean. The coefficient of variation in the simulated data used in this work is presented in Fig. A.8(b). We see that the variation of the modal model data decreases with increasing frequency, as expected, because the number of oblique modes increases. The Helmholtz data exhibit similar trends but also noticeable differences. The lowest variation is found for the Helmholtz data of the measured empty reverberation chamber (Section 6.2, Fig. 7(c)). This is not surprising, since the room has been designed to be diffuse and the wall impedance is uniform. The variation of the Helmholtz data of the simulated reverberation chamber (Section 5.2, Fig. 4(a)) is lower than that of the modal model data. Since this room is ergodic, this observation is reasonable. The Helmholtz data of the measured occupied reverberation chamber (Section 6.2, Fig. 7(d)) has the greatest variation. In this case, the impedance is non-uniform, leading to greater variation in modal decay times.

In this study, instead of using all eigenvalues found in a frequency band to calculate the reverberation time, we have used a limited set of eigenvalues. This is necessary due to the computational cost of computing all of the eigenvalues. In rooms with highly non-uniform impedance, using a limited set of eigenvalues might lead to inaccurate reverberation

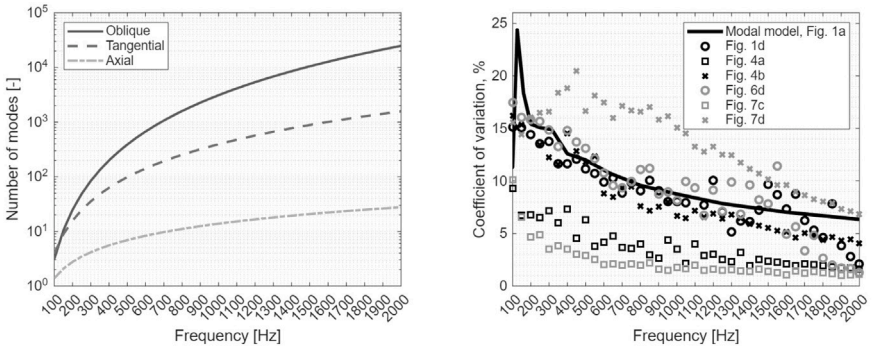

(a) Number of modes (b) Coefficient of variation

Fig. A.8. Variation of the reduced Helmholtz model solutions as a function of frequency.

times due to large variations in the modal decay times. However, based on the physical understanding of the modal decay time variation with frequency and the qualitative agreement between the coefficient of variation of the data, the use of a reduced set of Helmholtz solutions appears to be valid in this work.

Data availability

The authors do not have permission to share data.

References

[1] International Organization for Standardization. ISO 3382-2:2008 Acoustics — measurement of room acoustic parameters — part 2: reverberation time in ordinary rooms. International Organization for Standardization; 2008.

[2] International Organization for Standardization. ISO 354:2003 Acoustics — measurement of sound absorption in a reverberation room. International Organization for Standardization; 2003.

[3] Sabine WC. Collected papers on Acoustics. Cambridge: Harvard University Press; 1922.

[4] Badeau R. Statistical wave field theory. J Acoust Soc Am 2024;156(1):573–99. https://doi.org/10.1121/10.0027914

[5] Badeau R. Statistical wave field theory: special polyhedra. J Acoust Soc Am 2025;157(3):2263–78. https://doi.org/10.1121/10.0036254

[6] Badeau R. Statistical wave field theory: curvature term. J Acoust Soc Am 2025;157(3):1650–64. https://doi.org/10.1121/10.0036053

[7] Badeau R. Statistical wave field theory: anisotropic wave fields under neumann's boundary condition. J Acoust Soc Am 2026;159(3):2265–80. https://doi.org/10.1121/10.0042450

[8] Eyring CF. Reverberation time in "dead" rooms. J Acoust Soc Am 1930;1(2A):217–41. https://doi.org/10.1121/1.1915175

[9] Nowoświat A, Olechowska M. Investigation studies on the application of reverberation time. Arch Acoust 2016;41(1):15–26. https://doi.org/10.1515/aoa-2016-0002

[10] Jean-Dominique P. Revisiting reverberation. Acta Acust 2025;9:30. https://doi.org/10.1051/aacus/2025010

[11] Hodgson M. When is diffuse-field theory applicable? Appl Acoust 1996;49(3):197–207. https://doi.org/10.1016/S0003-682X(96)00010-2

[12] Stephenson UM. A rigorous definition of the term "diffuse sound field"–and why the sabine reverberation formula is different from the eyring formula. Fortschritte der Akustik-DAGA 2012 2012:541–2. https://pub.dega-akustik.de/DAGA_2012/data/articles/000401.pdf.

[13] Nolan M. Experimental characterization of the sound field in a reverberation room [Ph.D. thesis]. Technical University of Denmark; 2019.

[14] Martellotta F. Do we still need diffuse field theory? Canadian Acoustics 2019;47(1):19–28. https://jcaa.caa-aca.ca/index.php/jcaa/article/view/3269.

[15] Jacobsen F, Roisin T. The coherence of reverberant sound fields. J Acoust Soc Am 2000;108(1):204–10. https://doi.org/10.1121/1.429457

[16] Polack J-D. Modifying chambers to play billiards: the foundations of reverberation theory. Acta Acust united Ac 1992;76(6):256–72.

[17] Polack J-D. Playing billiards in the concert hall: the mathematical foundations of geometrical room Acoustics. Appl Acoust 1993;38(2):235–44. https://doi.org/10.1016/0003-682X(93)90054-A

[18] Joyce WB. Sabine's reverberation time and ergodic auditoriums. J Acoust Soc Am 1975;58(3):643–55. https://doi.org/10.1121/1.380711

[19] Schroeder MR, Kuttruff KH. On frequency response curves in rooms. Comparison of experimental, theoretical, and monte carlo results for the average frequency spacing between maxima. J Acoust Soc Am 1962;34(1):76–80. https://doi.org/10.1121/1.1909022

[20] Morse PM, Bolt RH. Sound waves in rooms. Rev Mod Phys 1944;16:69–150. https://doi.org/10.1103/RevModPhys.16.69

[21] Kuttruff H. Room Acoustics. 6th ed. CRC Press; 2017.

[22] Prinn AG. A review of finite element methods for room Acoustics. Acoustics 2023;5(2):367–95. https://doi.org/10.3390/acoustics5020022

[23] Picaut J, Simon L, Polack J-D. A mathematical model of diffuse sound field based on a diffusion equation. Acta Acust united Ac 1997;83(4):614–21.

[24] Prinn AG, Habets EAP. Diffusion equation-based estimation of spatially non-uniform surface absorption coefficients. In: Forum acusticum. Malaga, Spain; 2025. https://doi.org/10.61782/fa.2025.0300

[25] Jing Y, Xiang N. On boundary conditions for the diffusion equation in room-acoustic prediction: theory, simulations, and experiments. J Acoust Soc Am 2008;123(1):145–53. https://doi.org/10.1121/1.2805618

[26] Paris ET. On the coefficient of sound-absorption measured by the reverberation method. Lond Edinb Dubl Phil Mag 1928;5(29):489–97. https://doi.org/10.1080/14786440308565092

[27] Prinn AG, Tuna Ç, Walther A, Habets EAP. A study of the spatial non-uniformity of reverberation time at low frequencies. Appl Acoust 2025;227:110220. https://doi.org/10.1016/j.apacoust.2024.110220

[28] Fichera I, Van hoorickx C, Hornikx M. An empirical diffusion coefficient function for the acoustic diffusion equation model in long rooms. Appl Acoust 2026;246:111234. https://doi.org/10.1016/j.apacoust.2026.111234

[29] Farina A. Simultaneous measurement of impulse response and distortion with a swept-sine technique. In: Proceedings of AES convention 108. AES; 2000, no. 5093. https://secure.aes.org/forum/pubs/conventions/?elib=10211.

[30] Schroeder MR. New method of measuring reverberation time. J Acoust Soc Am 1965;37(3):409–12. https://doi.org/10.1121/1.1909343

[31] MATLAB. Version 9.3 (R2017b). Natick, Massachusetts: The MathWorks Inc.; 2017.